Short communication

Effects of cathode flow fields on direct methanol fuel cell-simulation study

Guo-Bin Jung*, Ay Su, Cheng-Hsin Tu, Yur-Tsai Lin, Fang-Bor Weng, Shih-Hung Chan

Fuel Cell Center, Yuan Ze University 135 Yuan-Tung Road, Chung-Li, Tao Yuan 320, Taiwan, ROC
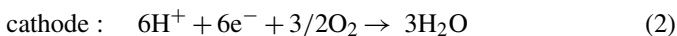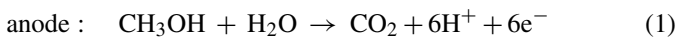
Abstract

Flow-field design of direct methanol fuel cell (DMFCs) plays an important role affecting the cell performance. Previous studies suggest that the combination of anode parallel flow field and cathode serpentine flow-field present the best and stable performance. Among these, cathode flow-field holds higher influence than that of anode. However, more detailed experiments needed to be done to find out the reasons. In this study, CFDRC half-cell models are adopted to simulate the flow phenomena within serpentine, parallel and grid flow field. We find that gas is well distributed within serpentine flow field while barren region are observed within parallel flow field. These factors contribute to the cell performance greatly. In addition, the durability test of DMFCs using parallel flow field is improved when the flow rate is increased or the current is uphold at inferior, so the barren region maintained at an acceptable level.
© 2007 Elsevier B.V. All rights reserved.

Keywords: Direct methanol fuel cell (DMFC); Flow field; barren region

1. Introduction

Methanol is an attractive fuel because its energy density is much higher than that of hydrogen, and it is an inexpensive liquid that is easy to handle, store and transport. A thermodynamic reversible potential for a methanol oxygen fuel cell is 1.21 V at 25 °C [1]. In the DMFC, methanol is oxidized at anode and oxygen is reduced at cathode. Carbon dioxide (CO_2) and water are produced according to the following electrochemical half-cell-reactions:

$$\text{anode}: \quad CH_3OH + H_2O \rightarrow CO_2 + 6H^+ + 6e^- \tag{1}$$

$$\text{cathode}: \quad 6H^+ + 6e^- + 3/2O_2 \rightarrow 3H_2O \tag{2}$$

which can be combined together to give the overall reaction as

$$CH_3OH + 3/2O_2 \rightarrow 2H_2O + CO_2 \tag{3}$$
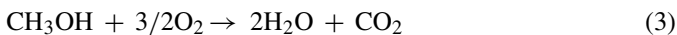
Thus, the overall cell reaction is the electro-oxidation of methanol to CO_2 and water. Apparently, the overall reaction produces CO_2 gas at the anode and liquid water at the cathode, should be removed from the electrode structure and cell as efficiently as possible to maintain an effective continuous reaction.

Like the water management at the cathode, the efficient removal of CO_2 at the anode is one of the most important research issues in the development of DMFCs.

Visual investigations of the CO_2 (g) evolution and flow behavior with flow beds are based on stainless steel plate and mesh [2–5]. According to their works a number of the flow designs are based on stainless plate and mesh, showed promising behavior in terms of gas removal characteristics and electrical performance.

To ensure free access for reactants to the electrodes especially at high current density, products have to be removed from the active surface area and out of the cell. This removal is achieved via diffusion layers and flow channels manufactured into the plates. The main tasks of these flow-field plates are to act as current-collectors and to guarantee distribution of fuel or air over the reaction surface area as well as removal of products from the cell. Nowadays, a few investigations have been extended to the reactant flow fields [6–9].

Currently, symmetrically grid, serpentine and parallel flow-fields (GFFs, SFFs, PFFs) are mainly used for both anode and cathode to facilitate mass transport to and from the active surface area. Due to long channels, serpentine flow-fields feature high pressure drops between the inlet and the outlet and result in large parasitic energy demands.

These result in large parasitic energy demands. Especially in the case of small, portable fuel-cell systems, the energy required to transport the fluids should be as small as possible. Flow-fields

---

* Corresponding author. Tel.: +886 3 4638800x2469; fax: +886 3 4555574.
E-mail address: guobin@saturn.yzu.edu.tw (G.-B. Jung).

Nomenclature

D_{O_2}	diffusion coefficient (8.39E−006 m^2 s^{-1})
F	Faraday constant (96,487,000 C kmol^{-1})
M_{O_2}	molecular weight of oxygen
Y_c	gas concentration of inlet

Greek letters

α	transfer coefficient
Δx	Thickness of diffusion layer (0.2 mm)
ε_d	diffusion layer effective porosity (0.4)
η	surface overpotential of catalyst layer
τ_c	catalyst tortuosity (1.5)
κ	reaction rate constant (kmol m^{-3} s^{-1})
ρ	density of oxygen (1.43 kg m^{-3})

with grid and parallel channels exhibit lower pressure differences, but inhomogeneous reactant gas-distribution can easily occur.

The effect of methanol crossover has attracted attention worldwide. Many factors, such as membrane material and modification, membrane thickness, methanol concentration, cell temperature and the pressure of cathode reactant have been investigated [10–13]. Besides intense studies of the methanol crossover [10], several research teams investigated the anode flow characteristics, e.g. by volume flow variation [14], carbon dioxide monitoring or flow bed characterization [15]. Most research efforts have been focused on the developing novel catalysts and new membrane for solid electrolyte [16–18]. However, issues concerning about the thermal and fluid flow in DMFCs should also be studied [19–22]. Several research groups have developed models related to the thermal management and flow characteristics in the liquid feed DMFCs [23–25]. Products of the electrochemical reactions, such as water and carbon dioxide can clog single cell channels [25,26]. As previously reported in several publications [27–31] flow-field design has a high influence on the performance stability of PEMFCs and DMFCs.

2. Experimental

Membrane-electrode assemblies (MEAs) were purchase from Lynntech. The MEAs are electrode coated membrane composed two gas diffusion layer. The gas diffusion layers are E-Tek ELAT GDL LT 2500-W for anode and ELAT GDL LT 2500-W for cathode. The catalyst loading on the anode side is 4 mg Pt–Ru cm^{-2}, while the catalyst loading on the cathode side is 4 mg Pt cm^{-2}. The active area for both anode and cathode are 25 cm^2.

Three different flow-fields are milled into the graphite composite material SIGRACET® BPP5 from SGL Technologies GmbH (SGL). The three different flow-field designs including GFF, SFF and PFF are presented in Fig. 1. The flow-field plates are 6.5 mm thick, 100.0 mm wide and 100.0 mm long. All gas channels are 2.0 mm deep. The widths of the ribs are mostly 2.0 mm. The active area defined by the gasket is 25.0 cm^{-2}. To avoid corrosion, the current collectors are made of Cu plates and coated with Au film. As shown in Fig. 2, the single cell in this study includes one MEA, two flow-field plates, two rubber gaskets, and two current collectors. In addition, a tape heater is attached to the extension area to adjust the cell operating temperature to a desired value during the experiments.

The test system is designed by ElectroChem, Inc., which consists of one instrument system (SA890B) and one CompuCell GTR system (FCT 2000). The instrument system (SA890B) is made by Scribners Associates Inc. The Scribners Associates' SA890B series including electronic loads is computer controlled. This control system consists of a bank of semiconductor devices conducting a large amount of current, equal to or greater than the fuel cell output. Before the performance test, a nitrogen (N$_2$) tank is opened using the control system to purge the impurities within the flow piping and the cell. Reactant flow rates are 5 and 150 ml min^{-1} for the methanol solution and pure oxygen respectively. Methanol is mixed with water, and the solution is pumped into the cell by a micropump (Micropump Inc., Vancouver, WA) while the O$_2$ flow rates are preset using the flow controller within the CompuCell GT® system made by MKS Instruments Inc. The methanol crossover current density is measured using an electrochemical oxidation technique.

3. Half-cell simulation theory

To simplify and save the time of set up of the simulation model, the User Scalar mode of CFDRC is used to simulate the oxygen consumption in flow fields and diffusion layer. The User Scalar transport equation as

$$\frac{\partial \rho \phi}{\partial t} + \nabla(\rho \vec{V})\phi = \nabla(D\nabla\phi) + S_\phi \tag{3-1}$$
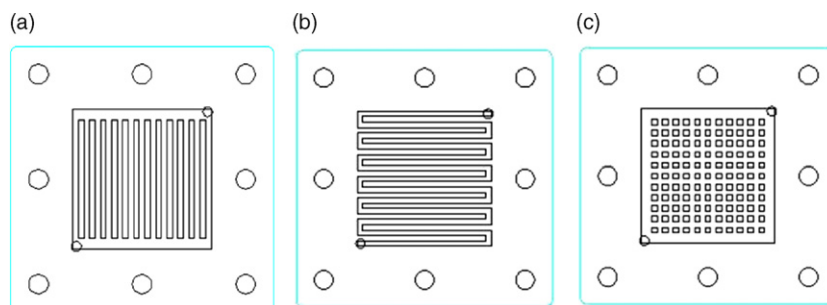

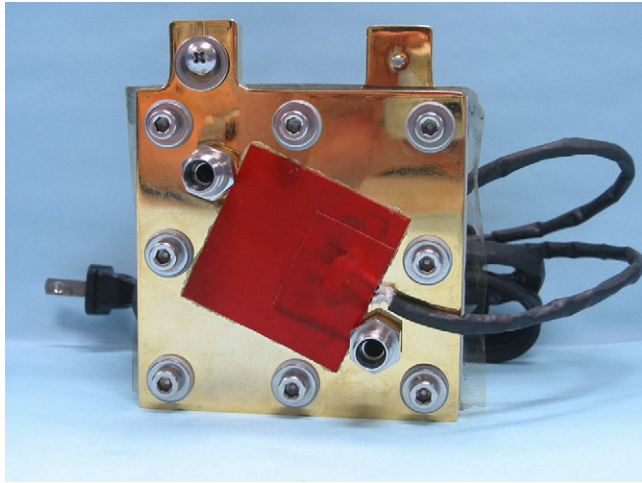Fig. 1. Investigated flow-fields for DMFC. (a) Parallel, (b) serpentine, and (c) grid.

Fig. 2. Schematic of 25 cm^2 DMFC single cell.

3.1. Half-cell catalyst layer equation

Half-cell simulation is based on Gurau [32] and Chu [33]. The oxygen consumption equation of catalyst layer is as follow:

$$\frac{d}{dx}\left(\varepsilon^{\tau_c}\rho D_{O_2}\frac{dY_c}{dx}\right) = \frac{j}{4F}M_{O_2} \tag{3-2}$$

where

$$j = 2F\kappa Y_c\, e^{(2\alpha F\eta/RT)} \tag{3-3}$$

$$\rho = \frac{PM}{RT} \tag{3-4}$$

The models of this study are including flow fields and catalyst, base on the above equation the equation becomes:

$$\varepsilon_c^{\tau_c}\rho D_{O_2}\frac{dY_c}{dx} \approx \frac{1}{2}M_{O_2}\kappa\,\Delta x\, e^{(2\alpha F\eta/RT)}Y_c \tag{3-5}$$

Then rearrange becomes:

$$D_{O_2}\frac{dY_c}{dx} = \frac{M_{O_2}\kappa\Delta x}{2\varepsilon_c^{\tau_c}\rho}e^{(2\alpha F\eta/RT)}Y_c \tag{3-6}$$

3.2. Half-cell catalyst boundary condition

Base on CFDRC, the boundary diffusion layer gas concentration equation of diffusion layer can be represented as

$$aD_{O_2}\frac{dY_c}{dx} + bY_c = c \tag{3-7}$$

Due to the models only build the diffusion layer and flow field, the diffusion layer boundary condition must equal to with the consumption of oxygen in catalyst layer. So arrange Eqs. (3)–(7) to fit with the form of Eqs. (3)–(6), then $a = 1$, $c = 0$ and the equation becomes:

$$D_{O_2}\frac{dY_c}{dx} = bY_c \tag{3-8}$$

Compare the Eqs. (3)–(5) and (3)–(8) the get Eqs. (3)–(9) as

$$b \approx \frac{M_{O_2}\kappa\Delta x}{2\varepsilon^{\tau_c}\rho}e^{(2\alpha F\eta/RT)} \tag{3-9}$$

Base on Eqs. (3)–(9) substitute η can get the value b, and then we can simulate the oxygen consumption of the whole cell reaction by transforming the boundary condition of diffusion layer to oxygen consumption.

4. Result and discussion

4.1. Contact resistance of different flow-field combinations

The influence of different flow-field combinations on the performance of the DMFCs is investigated. Different flow-field combination has different resistance due to non-equal contact area between the electrode and the flow-field plate. This will result in a wrong explanation of the influence of flow-field structure on the mass transfer and drainage of flow fields. Therefore, the priority of this section is to obtain the contact resistance of the different flow-field combinations. As shown in Table 1, different fabricating torque and combinations result in different contact resistance. It is obvious that increasing the fabricating torque gradually lower the contact resistance for all combinations. To prevent over-compression of the gas diffusion layer which can further influence the mass transport of reactants and products in addition to the flow-field plates, the fabricating torque of the cell is maintained at 20 kgf cm as constant for every combination. Among all combinations, the biggest difference of different combinations at 20 kgf cm torque is 0.3 mΩ and then that influence the power of cell is only 0.432 mW cm^{-2} under a constant load of 6A. Therefore, the effect of contact resistance due to different flow-field combinations on the cell performance can be neglected.

4.2. Effect of cathode flow-field design

The design of the cathode flow-field affects the air mass transfer and the drainage. If the product water is not removed from the cathode at a sufficient rate, flooding may occur and transport of reactants is hindered [34]. Ren et al. [35] and Mench et al. [36] have also mentioned that the overall DMFC performance is mainly determined by the cathode flooding. In DMFCs, the flooding water is producing by electrochemistry at cathode and crossover from anode.

Fig. 3 shows the polarization and power density curves different cathode flow-fields and parallel flow fields in anode at 70 °C. As shown in Fig. 3, the best DMFCs performance can be obtained when the serpentine flow field is used for cathode

Table 1
Summary of resistance of different torques and flow-field combinations (mΩ)

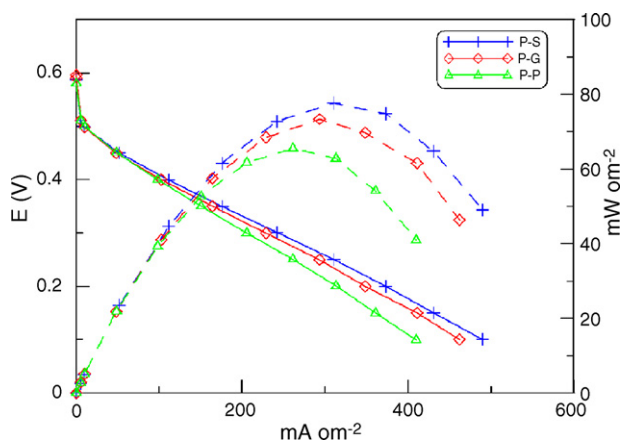| Combination	P–P	P–G	P–S
Resistance (mΩ) of 15 kgf cm	1.04	1.2	1.47
Resistance (mΩ) of 20 kgf cm	0.9	1	1.2
Resistance (mΩ) of 30 kgf cm	0.76	0.75	0.98

Fig. 3. I–E characteristics of a DMFC operating with different flow-fields on cathode and parallel on anode (70 °C, O_2 150 cm³ min⁻¹, MeOH (2 M) 5 cm³ min⁻¹) (anode–cathode).

Fig. 5. Simulation model domain.

side. However, with the parallel flow field shows the worst one. By virtue of the pressure-driven mass flow in the channels, the removal of this water is eased by a serpentine structure. In addition, the removal of the water results in the replacement of fresh air which leads to a higher performance depressing the sluggish mass transfer limitations. In the parallel design, air and water in the cathode can frequently flowing through the one or more channels. This reduces the reactant flow and some of the flow channels of parallel designs are by passed; subsequently the total active surface area loses the performance to provide sufficient amount of power. In the grid design, due to the vertical inlet of flow and the flow-field characteristic, the flow of the reactant becomes turbulent which leads to more uniform distribution than in parallel design.

The long-term behavior of the output voltage of the flow-field designs have been investigated by 150 min tests at a constant-current discharge as shown in Fig. 4. At first, the cells are operated for 30 min at 2A, corresponding to 80 mA cm⁻². Subsequently the cell currents increased to 4, 6, 8, and 10A, or 160, 240, 320 and 400 mA cm⁻² (The parallel flow field is operated

only till 8A). For all stages, the serpentine flow-field presents the highest cell voltage. In low current loading (2, 4 A), there are less differences in the output voltages of different cathode flow fields. However, in higher current (6, 8, 10 A) operation, the difference between the serpentine and grid are more obvious due to the mass transfer of oxygen and removal of the produced water. In the parallel flow-field design, an oscillating output voltage is observed. As the current increases, the oscillating effect intensifies and the performance becomes more unstable. At 8 A, the voltage cannot be maintained and is interrupted within minutes. This is due to the barren region of flow field and water accumulation leading to the mass transport limitation.

To determine the accurate influences of the cell performance with the flow-field designs, the half-cell reaction simulations are performed and the oxygen distributions of different flow-field design are investigated.

4.3. Flow-fields half-cell simulation

The reactant gas flow distribution is simulated using the CFDR half-cell reaction simulation models to determine the different characteristics of the flow fields. Fig. 5 shows the domain of the simulation. The gas flow direction is as shown in Fig. 5. Oxygen enters vertically to the flow filed along the Z axis and turns to Y axis at gas diffusion layer surface. In this study, by using three different oxygen consumption value B, we can simulate two different operations current. For high current operation the value of B is 0.01 and for low current operation the value of B is 0.001. Figs. 6–8, shows that for low current operation, the mass fraction of flow fields is not much different in serpentine and grid designs. The parallel design has worse gas distribution than others, so the performance is lower.

Figs. 9–11 are the mass fraction profiles at the interface of catalyst layer and gas diffusion layer with three different flow-field designs at high current loading. We can see the oxygen concentration distribution with different flow-field designs at high current operation.
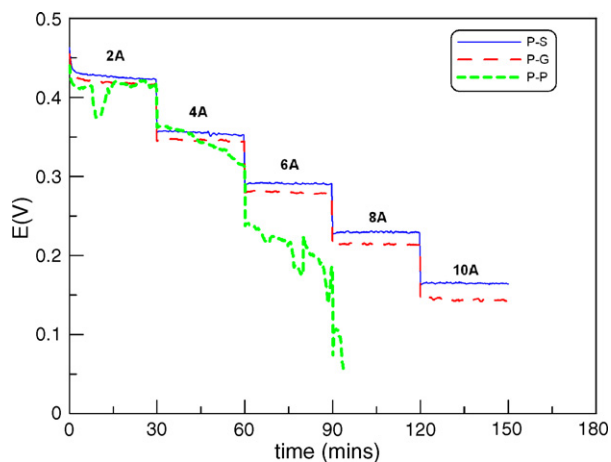

Fig. 4. Constant-current discharge performance of DMFCs with different flow-fields on cathode and parallel on anode. The cells are operated at a total current density of 2, 4, 6, 8, and 10 A (anode–cathode) (S, serpentine; G, grid; P, parallel).
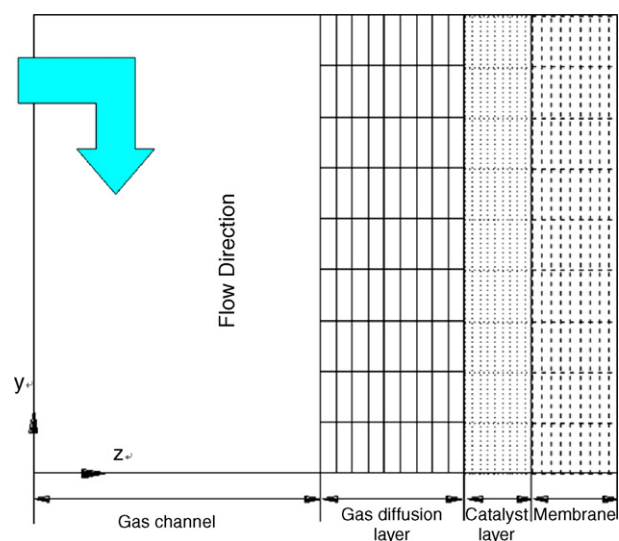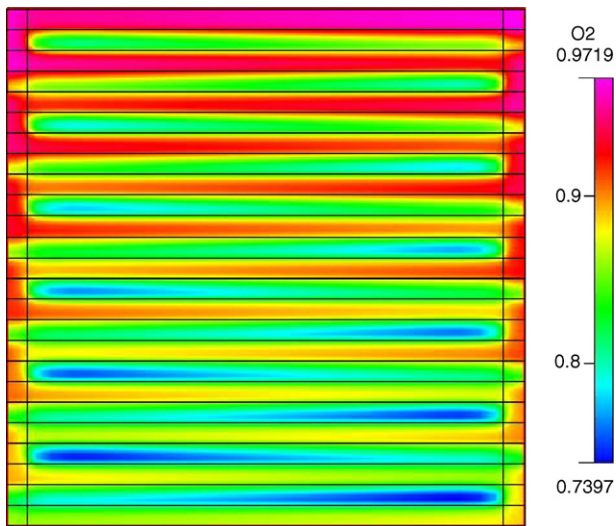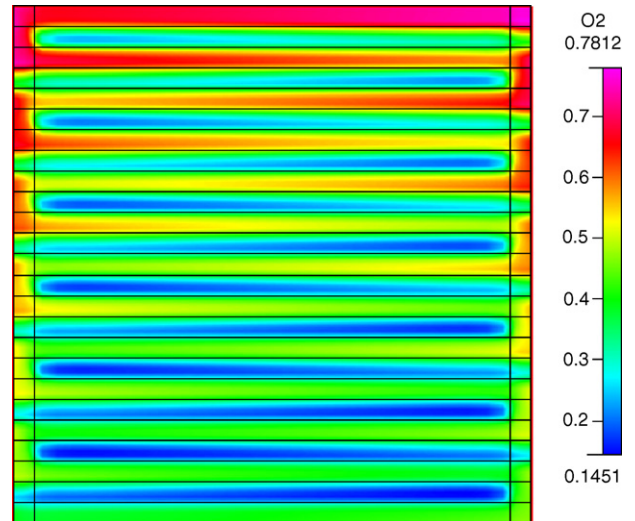
Fig. 6. Oxygen mass fraction at low current operation with serpentine flow-field design.
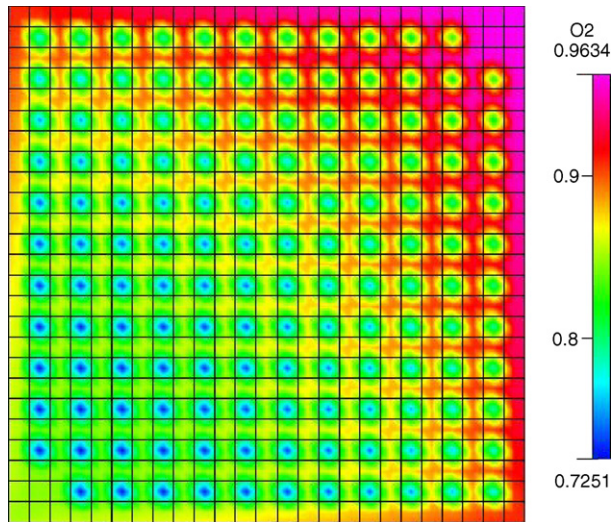

Fig. 7. Oxygen mass fraction at low current operation with grid flow-field design.
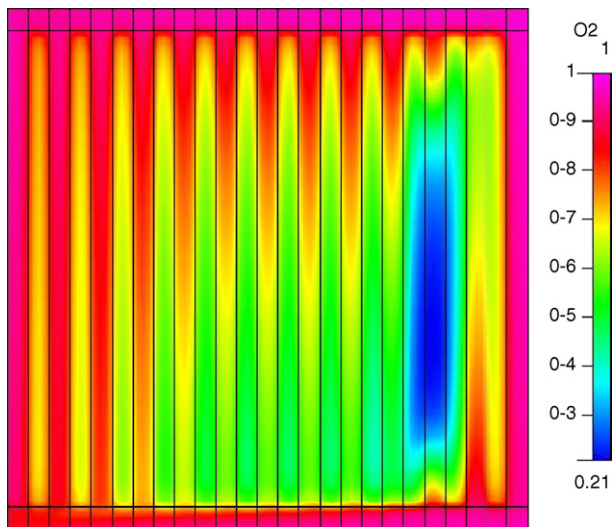

Fig. 8. Oxygen mass fraction at low current operation with parallel flow-field design.
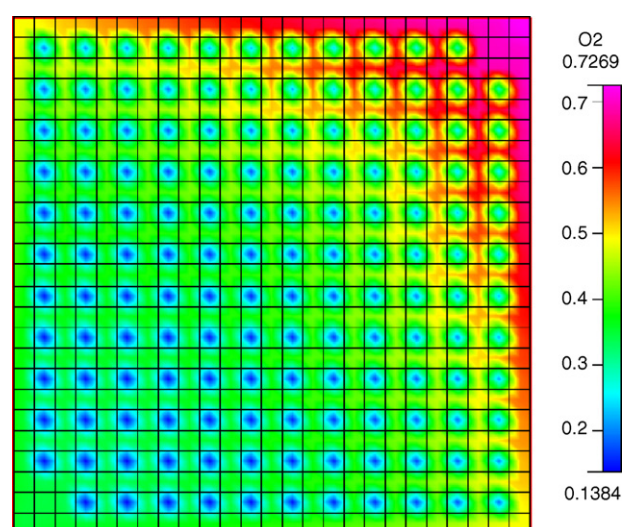

Fig. 9. Oxygen mass fraction at high current operation with serpentine flow-field design.

For the serpentine design, all of the oxygen and water have to flow through the only channel. Therefore, oxygen and water may flow in one or more of the many channels in the parallel and grid designs. This can result in areas with no reactant flow, so at high current operation they can not provide enough reactant gas and remove the water. But for the grid design, due to the vertical gas flow entrance of the flow field and the raise of columns lead reactant flows become turbulent. That is why the grid design can provide better gas distribution than that of the parallel design.

But for parallel flow field, the bad distribution due to free roaming areas of gases causes barrenness such as show as Figs. 8–11 The barren region results in flooding water (which is produced by electrochemistry at cathode and crossover from anode) that cannot be removed in time during high current operation. Finally it leads to a decrease in cell performance and stability. Similar results have been obtained for other flow-fields with a non-forced flow direction [37]. It can be used to prove

Fig. 10. Oxygen mass fraction at high current operation with grid flow-field design.
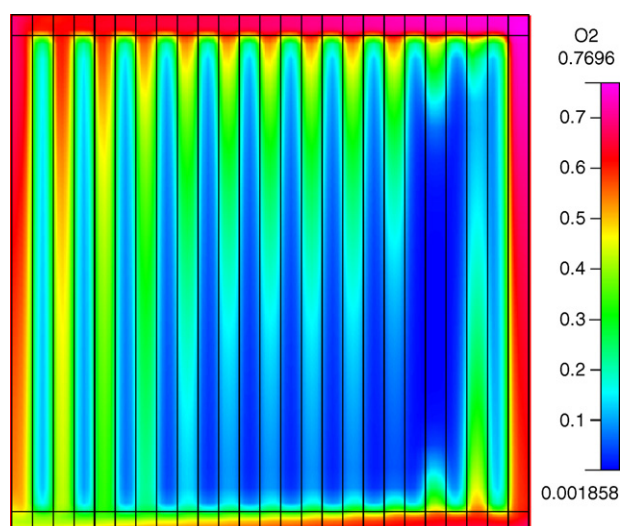
Fig. 11. Oxygen mass fraction at high current operation with parallel flow-field design.

the performance of parallel flow-field design at higher current loading in Fig. 4.

5. Conclusion

In this study, the effect of gas flow-field design on the performance DMFCs has been investigated. It has been shown that various structures have a large impact on the stability of fuel-cell operation due to their different ability to provide fuel and remove produced water, respectively.

The flow distribution in fuel cells has an important influence on the power density. Due to additional flow paths offered by the diffusion layer, even a serpentine structure can inhomogeneously distribute the reactants across the flow-field area. The relationship between the fuel distributions and the performance is shown by simulation and experimental results.

In the cathode side, the serpentine flow-field design has well mass transfer ability and can exclude water due to higher pressure-drop, so the serpentine flow-field performs better and has more stable performance. Oxygen and water may flow in one or more of the channels in the parallel and grid designs. Therefore inhomogeneous flow distribution occurs and parts of the catalyst surface are bypassed. But for the grid design, due to the vertical gas flow entrance to the flow field and the raise of the columns which lead the reactant flows to become turbulent, the grid design can provide better gas distribution than the parallel design. In the parallel flow-field design, an oscillating output voltage is observed. As the current increases, the oscillating effect intensifies. For high current operation, the performance decrease rapidly and be interrupted due to the bad distribution of reactant and that cannot remove flooding water in time, this in turn leads to inactive regions. The effects obtained by simulation studies have been proven by experiments.

In overall appraisal, the DMFCs with serpentine design on cathode show the best performance and have the highest stability.

References

[1] K. Kordesch, G. Simader, Fuel Cells and Their Applications, VCH, Weinheim, 1996.
[2] H. Yang, T.S. Zhao, Electrochim. Acta 50 (2005) 3243–3252.
[3] H. Yang, T.S. Zhao, Q. Ye, J. Power Sources 139 (1–2) (2004) 79–90.
[4] K. Scott, W.M. Taama, P. Argyropoulos, J. Power Sources 79 (2001) 43–59.
[5] K. Scott, P. Argyropoulos, P. Yiannopoulos, W.M. Taama, J. Appl. Electrochem. 31 (2001) 823–832.
[6] T.V. Nguyen, J. Electrochem. Soc. 143 (1996) L103–L105.
[7] D.L. Wood, J.S. Yi, T.V. Nguyen, Electrochim. Acta 43 (1998) 3795–3809.
[8] L. Liu, C. Pu, R. Viswanathan, Q. Fan, R. Liu, E.S. Smotkin, Electrochim. Acta 43 (1998) 3657–3663.
[9] J.S. Yi, T.V. Nguyen, J. Electrochem. Soc. 146 (1999) 38–45.
[10] A. Heinzel, V.M. Barragan, J. Power Sources 84 (1) (1999) 70–74.
[11] J. Cruickshank, K. Scott, J. Power Sources 70 (1998) 42–46.
[12] I. Valdez, S.R. Narayanan, Electrochem. Soc. Proc. 98 (27) (1998) 382.
[13] A. Kuver, W. Vielstich, J. Power Sources 74 (1998) 211–218.
[14] K. Scott, W.M. Taama, S. Kramer, P. Argyropoulos, K. Sundmacher, Electrochim. Acta 45 (1999) 945–957.
[15] P. Argyropoulos, K. Scott, W.M. Taama, Electrochim. Acta 44 (1999) 3575–3584.
[16] A.K. Shukla, J. Electroanal. Chem. 504 (2001) 111–119.
[17] P. Dimitrova, K.S. Dhathathreyan, J. Electroanal. Chem. 532 (2002) 75–83.
[18] K.D. Kreuer, J. Membr. Sci. 185 (2001) 25–39.
[19] K. Scott, W.M. Taama, P. Argyropoulos, J. Power Source 79 (1999) 43–59.
[20] H. Guo, C.F. Ma, M.H. Wang, et al., J. Eng. Thermophys. 25 (2004) 148–150.
[21] H. Guo, C.F. Ma, M.H. Wang, et al., in: R.K. Shah (Ed.), Proceedings of the First International Conference on Fuel Cell Science, Engineering and Technology, ASME, New York, 2003, pp. 471–476.
[22] H. Guo, C.F. Ma, M.H. Wang, Proceeding of the First Sino-German Workshop on Fuel Cell, DICP, Dalian, 2002, pp. O82–O86.
[23] K. Scott, P. Argyropoulos, K. Sundmacher, J. Electroanal. Chem. 30 (9) (2000) 1014–2006.
[24] Z.H. Wang, C.Y. Wang, J. Electrochem. Soc. 150 (4) (2003) A508–A519.
[25] K. Tüber, D. Pócza, C. Hebling, J. Power Sources 124 (2003) 403–414.
[26] Argyropoulos, K. Scott, W.M. Taama, Electrochim. Acta 44 (1999) 3575–3584.
[27] S. Oedegaard, R. Hufschmidt, C. Wilmshoefer, Second European Polymer Electrolyte Fuel Cell Forum, European Fuel Cell Forum, Oberrohrdorf, Lucerne, Switzerland, 30 June to 4 July, 2003.
[28] H. Bewer, T. Dohle, J. Beckmann, R. Mergel, D. Neitzel, Stolten, Proceedings of the First European Polymer Electrolyte Fuel Cell Forum European Fuel Cell Forum, Oberrohrdorf, Lucerne, Switzerland, July 2–6, 2001.
[29] Aricò, P. Cret'ı, V. Baglio, E. Modica, V. Antonucci, J. Power Sources 91 (2000) 202–209.
[30] Tüber, M. Zobel, H. Schmidt, C. Hebling, J. Power Sources 122 (2003) 1–8.
[31] Wilkinson, O. Vanderleeden, Handbook of Fuel Cells, vol. 3, John Wiley & Sons, Chichester, UK, 2003, pp. 315–324.
[32] V. Gurau, F. Barbir, H. Lin, J. Electrochem. Soc. 147 (2000) 2468–2477.
[33] H.S. Chu, C. Yeg, F. Chen, J. Power Sources 123 (2003) 1–9.
[34] J.J. Baschuk, X. Li, J. Power Sources 86 (2000) 181–196.
[35] X. Ren, S. Gottesfeld, J. Electrochem. Soc. 148 (2001) A87–A93.
[36] M. Mench, S. Boslet, S. Thynell, J. Scott, C.Y. Wang, The Electrochemical Society Proceedings Series, Pennington, NJ, 2001, p. 241.
[37] A. Oedegaard, S. Hufschmidt, R. Wilmshoefer, C. Hebling, Second European Polymer Electrolyte Fuel Cell Forum, 30 June to 4 July, European Fuel Cell Forum, Oberrohrdorf, Lucerne, Switzerland, 2003.